Progress In Electromagnetics Research C, Vol. 136, 101–112, 2023

Efficient Implementation of Aperture Fill Time Correction for Wideband Array Using the Low-Complexity Keystone Transform

Lin Wang[1], Yiyang Jiang[1, *], Yu Jiang[2], Baoli Tian[3], and Mingwei Shen[1]

Abstract—In order to remove the influence of the aperture fill time (AFT) for wideband array, the scaling principle of the Keystone (KT) transform is applied to eliminate the linear coupling between spatial domain and frequency domain of wideband array signal. However, the classic KT transform is implemented by interpolation Sinc which is difficult to apply in engineering and leads to the serious problem of insufficient data. To address this, a realization of the low-complexity KT transform is presented, and it is implemented using only the Chirp-z transform (CZT) and fast Fourier transforms (FFT). Additionally, an Autoregressive (AR) model is proposed to compensate the insufficient data for each range, and the order of AR is estimated by the rank of the signal covariance matrix. Simulation results demonstrate that the proposed algorithm significantly reduces computational burden and improves the performance of wideband array beamforming.

1. INTRODUCTION

Wideband phased arrays are the ideal choice for target identification and radar imaging for their high range resolution, and they provide key technical support for modern radars, thus the combination of signal processing techniques and wideband phased arrays has garnered significant attention. However, the aperture fill time (AFT) phenomenon [1–3], an inherent characteristic of wideband arrays, severely degrades beamforming performance. The time delay of the signal received by different array elements cannot be ignored as long as the signal is not vertically incident onto the array, resulting in that the range-compressed signal cannot be focused in the same range cell and cannot be coherently accumulated efficiently [4]. In the frequency domain, the AFT leads to deviation of steering vectors at different frequencies, which increases the computational complexity in the process of beamforming. Therefore, most narrowband signal processing algorithms cannot be directly applied in wideband array systems.

At present, two efficient algorithms for compensating the AFT have been widely used in signal processing. One of these methods is processed in the time domain which originates from the Finite Impulse Response (FIR) filter based on the tapped delay line proposed by Frost [5]. It is known that the time delay of the vertically incident signal and the error of array pointing are both zero, thus the signal can be regarded as a reference, and time delay of the non-vertically incident signal can be properly compensated to eliminate the AFT. The other method is processed in the frequency domain [6] which divides the incident signal into multiple subbands using filters and calculates the adaptive weights for each subband to perform narrowband beamforming. The wideband beamforming can be completed by integrating the processing results of all subbands. Relevant research results show that for the same incident signal, these two methods have similar performance when the number of filters in the time-domain algorithm is the same as the number of subbands in the frequency-domain processing [7].

Received 8 April 2023, Accepted 4 August 2023, Scheduled 14 August 2023
* Corresponding author: Yiyang Jiang (jyy_hhu1997@163.com).
[1] College of Computer and Information Engineering, Hohai University, Nanjing, China. [2] Unit 95438 of PLA Air Force, Meishan, China. [3] Science and Technology on Electronic Information Control Laboratory, Chengdu, China.

In engineering applications, the performance of these two compensation methods is limited by the filter order. A large amount of filters will increase the computational burden of the algorithm, and conversely, performance loss will be inevitable. However, the Keystone (KT) transform [8–10], known as an effective envelope alignment technique, has been widely used in the fields of radar target detection and target imaging. The KT transform can align all the frequency points of the wideband signal to the carrier frequency by preprocessing the signal in the frequency-spatial domain, which can effectively solve the problem caused by AFT. Sinc interpolation [11] is also a conventional method used to complete the scale transformation of the KT transform (KT-Sinc), but it is not suitable for engineering applications due to its difficulty in implementation. Therefore, this paper introduces a low-complexity KT transform based on the Chirp-z transform (CZT) algorithm (KT-CZT) [12–14]. For the wideband receiving array model, only the fast Fourier transforms (FFT) and z transform are needed to complete the whole process of scaling.

The conventional KT transform uses the carrier frequency as the reference frequency for scaling. However, when dealing with frequency-element signals, the data at frequency points lower than the carrier frequency suffer from insufficient data due to the expansion and contraction of sampling intervals in the spatial domain. To tackle this problem, this paper combines Autoregressive (AR) model [15] with the KT transform. In this way, after preprocessing the signal with the KT transform, the AR model can be applied to work out the insufficient data of array elements directly from the 2D time domain form of the signal.

The remainder of this paper is structured as follows. In Section 2, the basic model of the wideband receiving array is established, and the principle of the KT transform to correct the AFT is introduced. Meanwhile, the KT-CZT is applied into the wideband array, and the process of the CZT for spatial scaling is deduced. In Section 3, the proposed KT-CZT-AR algorithm is presented. The validity of our approach is confirmed through a simulation experiment in Section 4. Finally, we provide the conclusion of this paper in Section 5.

2. AFT CORRECTION USING THE KT-CZT

2.1. Principle of the KT Transform

In fact, Keystone transform is an effective processing method for the migration through range cell in high resolution radar imaging [16]. Assuming a uniform linear array (ULA) with M elements spaced at $d = \lambda/2$, receive a far-field wideband desired signal $d_0(t)$ and P independent wideband jamming signals from directions $\theta_0, \theta_1, \ldots, \theta_P$. The received signal sources $D(t) = [d_0(t), d_1(t), \ldots, d_i(t)]$, $i \in [0, P]$ and the channel noise $n(t)$ have no correlation, and the array manifold matrix of the received signal is $A = [a(\theta_0), a(\theta_1), \ldots, a(\theta_i)]$. The array output signal at time t in range can be expressed as

$$x(t) = AD(t) + n(t) = a(\theta_0)\, d_0(t) + \sum_{i=1}^{P} a(\theta_i) d_i(t) + n(t) \tag{1}$$

Considering that the desired signal is a linear frequency modulation (LFM) signal, and the range-compressed signal can be expressed by a time-element function as

$$y(t, n) = x\left(t - \frac{r_n}{c}, n\right) \exp\left(-j\frac{2\pi f_0}{c} r_n\right) \tag{2}$$

where f_0 represents the signal carrier frequency, and c is the speed of light. r_n denotes the wave range difference between the nth array element and the center array element. This paper takes the central array element as a reference, and the time delay for the signal to reach other array elements can be expressed as $r_n/c = nd \sin\theta_0/c$ ($n \in [-M/2, M/2 - 1]$).

The time delay causes sampling time deviations for the signals received by different elements from Equation (2). As a result, the range-compressed signal cannot be focused on the same range cell during simulation, which is known as the AFT. FFT transform is performed on (2), and its Fourier spectrum is

$$y(f, n) = x(f, n) \exp\left(-j\frac{2\pi f_0}{c} r_n\right) \exp\left(-j\frac{2\pi f}{c} r_n\right) \tag{3}$$

From Equation (3), it is evident that the exponential term $\exp(-j\frac{2\pi f}{c}r_n)$ shows a mutual coupling between the array element variable $n \in [1, M]$ and the range frequency variable $f \in [-B/2, B/2]$. This results in a signal steering vector of the array that varies with the instantaneous frequency. This coupling effect is also the root cause of the aperture effect.

The core of the KT transform is to introduce a virtual array element $\hat{n} = (f_0 + f)/f_0 * n$ to achieve the scaling transformation of the spatial domain, which is commonly implemented using Sinc interpolation. The number of interpolation orders used to calculate each new sampling point is represented by N, and the implementation of the KT transform can be expressed as follows:

$$y(f, \hat{n}) = y\left(f, \frac{f_0}{f_0 + f}\hat{n}\right) = \sum_{n=-N/2}^{N/2} y(f, n)\mathrm{sinc}\left(\frac{f_0}{f_0 + f}\hat{n} - n\right) = x(f, \hat{n})\exp\left(-j\frac{2\pi f_0}{c}d\hat{n}\sin(\theta_0)\right) \quad (4)$$

From Equation (4), it is evident that the instantaneous frequency no longer appears in the exponential term $\exp(-j\frac{2\pi f_0}{c}d\hat{n}\sin(\theta_0))$, effectively correcting the linear coupling between the range-frequency domain and the spatial domain. As a result, the wideband signal steering vector is only dependent on the carrier frequency, which is the same as the narrowband signal steering vector. Therefore, narrowband processing methods can be directly applied to wideband signals.

2.2. KT Transform Implemented by the CZT

In order to enhance the accuracy of the interpolated data, increasing the interpolation orders is a commonly employed method. However, this approach not only adds to the computational burden, but also exacerbates the issue of insufficient data resulting from truncating the interpolation kernel. Although we attempted to address this problem in [17], the proposed solution is still not well suited for engineering applications. Moreover, the low-frequency component of the KT-transformed signal can also suffer from insufficient data due to the expansion and contraction of the spatial sampling interval. The truncated interpolation kernel exacerbates this problem. On the other hand, using a shorter interpolation kernel may result in the occurrence of Gipps ringing and reduced interpolation accuracy. Therefore, considering the ease of implementation and computational efficiency, the KT-Sinc is not typically the primary choice for engineering applications.

As shown in Fig. 1(b), the CZT is sampled at equal intervals on the unit circle, and the z transform of each sampling point can be obtained as the Fourier transform of each sampling point. From the KT transform, both the input and output samples in range resampling are uniformly spaced to sample the spatial domain, so it is suitable for the application of the CZT. The number of array elements that need to be scaled in this paper is M, and the CZT is formulated through the following convolution

$$Y(f, z_k) = \sum_n y(f, n)\left(AW^{-k}\right) = W^{\frac{k^2}{2}} \cdot \left[y(f, n)A^{-n}W^{\frac{n^2}{2}}\right] \otimes W^{-\frac{n^2}{2}} \quad (5)$$

where $k \in [1, M]$, $\otimes$ represents the convolution, and $y(f, n)$ is the digitized sampled data of the signal in the frequency-spatial domain.

From (5), $A = A_0 e^{j\theta_0}$, $W = W_0 e^{-j\varphi_0}$, where A_0 controls the length of the vector radius of the initial sampling point, and θ_0 is the initial phase angle of the sampling point. For the implementation of the KT transform, $A_0 = 1$ and $\theta_0 = 0$ are generally taken. In addition, $W_0 = 1$ is the stretch rate of the spiral, and φ_0 is the frequency spacing between two adjacent sampling points in spatial frequency resampling. According to the scaling principle of the KT transform, φ_0 should be taken as $\frac{f_0+f}{f_0} \cdot \frac{2\pi}{M}$. Therefore, (5) can be rewritten as

$$\begin{aligned} Y(f, z_k) \;=\; & \exp\left(-j\frac{f_0 + f}{f_0} \cdot \frac{\pi k^2}{M}\right) \cdot \left[y(f, n)\exp\left(-j\frac{f_0 + f}{f_0} \cdot \frac{\pi n^2}{M}\right)\right] \\ & \otimes \exp\left(j\frac{f_0 + f}{f_0} \cdot \frac{\pi n^2}{M}\right) \end{aligned} \quad (6)$$

The convolution process in Equation (6) can be implemented through the use of Fast Fourier Transform (FFT) and matrix complex multiplication. As such, the implementation of the Chirp Z-Transform (CZT) can be summarized as follows:

1) A minimum integer L, which is an integer power of 2, is obtained to facilitate the calculation using FFT and makes it satisfy $L \geq 2M-1$.
2) Set the parameters shown in (6), and $AW = \exp(-j\frac{f_c+f}{f_c} \bullet \frac{2\pi}{M})$ can be obtained.
3) Construct sequences $g(f,n)$ and $h(f,n)$ of length L, and add zero-point values at the back end of $g(f,n)$, that is

$$g(f,n) = \begin{cases} y(f,n)\exp\left(-j\dfrac{f_0+f}{f_0}\cdot\dfrac{\pi n^2}{M}\right), & 0 \leq n \leq M-1 \\ 0, & M \leq n \leq L-1 \end{cases} \tag{7}$$

$$h(f,n) = \exp\left(j\frac{f_0+f}{f_0}\cdot\frac{\pi n^2}{M}\right), \quad 1-M \leq n \leq M-1 \tag{8}$$

4) The process of convolution shown in (6) can be completed by using L-point FFT and matrix complex multiplication

$$V(f,n) = IFFT\{FFT[g(f,n)] * FFT[h(f,n)]\} \tag{9}$$

5) Finally, the first M points of A are chosen as weights, that is

$$Y(f,z_k) = v(f,n)\exp\left(-j\frac{f_0+f}{f_0}\cdot\frac{\pi n^2}{M}\right), \quad 0 \leq n \leq M-1 \tag{10}$$

The entire process of the KT transform has been completed in (10). Once being processed by the CZT, the signal transitions from the spatial domain to the frequency domain, resulting in a two-dimensional frequency domain representation. To convert it back to the time-domain form, a two-dimensional Inverse Fast Fourier Transform (IFFT) is applied. Here, $y(t,\tilde{n})$ represents the time-domain form of the range-compressed signal, and $\tilde{n}$ is the sampling point of the array element domain after scaling.

Figure 1(a) shows the samples on the wavenumber axis of the CZT, where $\theta_{ref} = 0°$ is the reference angle, and θ and $-\theta$ are two signal sources impinging on the ULA. Due to the aperture effect, the spatial frequency corresponding to each range frequency of the wideband signal is different. As a result, the spatial frequency of the two signal sources appears linearly inclined. The interval between adjacent dotted lines in Fig. 1(a) represents the frequency interval of the spatial frequency corresponding to the

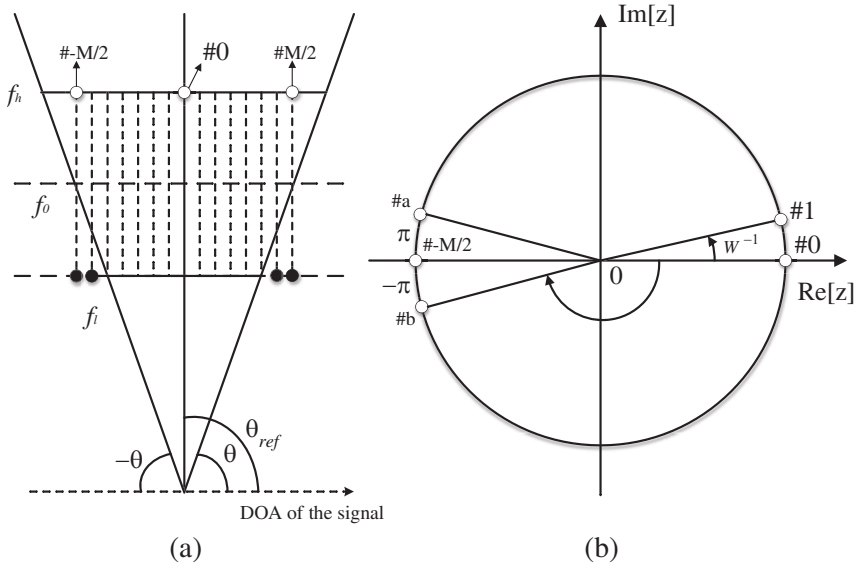

Figure 1. KT-CZT algorithm: (a) Samples on the wavenumber axis, (b) the CZT on the unit circle in the z-plane.

carrier frequency. Therefore, the CZT corrects the frequency interval of all range frequency points to be the same as the carrier frequency, thus removing AFT. Fig. 1(b) illustrates the CZT process on the unit circle in the z-plane. In order to detect the signals of various angles effectively, the sampling point range of the array element is set to $[-M/2, M/2]$. In Fig. 1(b), point $\#M/2$ and point $\#-M/2$ are coincident; point #0 is the start point of sampling; and W^{-1} represents the sampling interval of spatial frequency. It can be seen clearly from the transformation process of point $\#-M/2$, points #a and #b are the spatial frequency sampling points corresponding to the resampling of the highest range frequency and the lowest range frequency after the KT transform, respectively. In Fig. 1(a), the spatial frequency interval corresponding to the highest range frequency has decreased after the CZT, and this situation is opposite of the lowest range frequency. Therefore, the KT transform based on the CZT algorithm can effectively solve the problem of unequal spatial frequency of different ranges, thereby correcting the AFT.

3. KT-CZT-AR ALGORITHM

The conventional KT transform typically uses the carrier frequency as the reference frequency. Therefore, in the wideband system, the steering vectors for frequencies other than the carrier frequency are corrected by the KT transform and become equivalent to the steering vector for the carrier frequency. The KT transform can correct the AFT by resampling to adjust the spatial sampling interval. However, as shown in Fig. 1, the spatial frequency for frequencies lower than the carrier frequency will be expanded, as indicated by the solid circle in Fig. 1(a). This, in turn, leads to a shrinking of the time domain sampling axis of the array element, and the edge elements of the array axis may experience insufficient data. To address this issue, the AR model can be applied to compensate the insufficient data in the array element.

3.1. Principle of AR Model

The array system in this paper consists of a wideband linear array, resulting in a received signal with noticeable time correlation. The same signal received by different array elements exhibits only a linear delay, which is compensated for after the KT transform. Given this setup, the AR model can effectively address the insufficient data of the array elements.

This paper utilizes the backward prediction method to predict the insufficient data, that is

$$y\left(t,\tilde{n}\right)=\sum_{i=1}^{P}\alpha_i y\left(t,\tilde{n}-i\right)+\varepsilon_t \tag{11}$$

where α_i is the AR model coefficient, and P and ε_t represent the model order and model error, respectively. The forward prediction model uses the past time series $y\left(t,\tilde{n}-i\right),\ i\in[1,P]$ of the sampled signal and the correlation between them to predict the current state $y\left(t,\tilde{n}\right)$ of the system.

In this paper, the signal data is compensated in the two-dimensional time domain by using AR model. Specifically, the number of array elements experiencing insufficient data in each range cell can be expressed as

$$N_l=\frac{B}{2f_0}M \tag{12}$$

Currently, the order of the AR model and its coefficients are typically determined using the Akaike information criterion (AIC), Bayesian modification of AIC criterion (BIC), and the Burg algorithm [18, 19]. In this paper, the AIC criterion is utilized, which is based on the concept of entropy, to estimate the number of points. Its model can be defined as

$$\mathrm{AIC}\left(k\right)=N\ln\sigma_k^2+2k \tag{13}$$

where k represents the order of the AIC model, and σ_k^2 denotes the error in predicted power of the k-order AR model. As the order k increases, $2k$ increases as well, but σ_k^2 decreases. By varying the value of k, the minimum value of AIC(k) can be obtained, and this value will represent the order of the model determined by the criterion. According to the order P of the AR model, the time series

$Y(t,\tilde{n}) = [y(t,0), y(t,1), \ldots, y(t,M-1)]$ of each range cell can be used to represent the element data for each range cell, and $y(t,\tilde{n}-N_l-i)$, $i \in [1,P]$ of this time series can be used to restore the element data. Finally, once the recovered data is considered known, the recovery process can proceed recursively in reverse order to recover all insufficient data. The entire process of recovering element data can be expressed as

$$y(t,\tilde{n}-N_l+1) = \sum_{i=1}^{P} \alpha_i * y(t,\tilde{n}-N_l-i+1) \tag{14}$$

3.2. Order Estimation based on the Rank of Covariance Matrix

In a wideband system, the incident signal contains not only the target signal but also various jamming signals and channel noise. Choosing a small model order can negatively impact the recovery effectiveness of the AR model, while a large order can increase the computational burden. Therefore, it is crucial to strike a balance between the value of the AR model order and the recovery performance of the signal data.

Supposing that k is the number of received signal sources, iterative operations conducted on potential "k" values. The optimal estimation of the number of sources can be obtained when the value of (13) is the smallest. Therefore, the AIC criterion serves as an information-theoretic method for estimating the number of sources. Additionally, based on this same property, the number of sources can be directly considered as the order of the recovery of the AR model. However, in the presence of channel noise and interference signals, the number of information sources becomes an uncertain value in aliasing signals, and the calculation burden increases if all possible values are calculated and compared repeatedly. Therefore, the number of information sources can be determined first through the feature decomposition of the covariance matrix, and the basic form of the reception of aliasing signals can be obtained through Formula (1). In order to obtain the exact rank of covariance matrix, rank estimation is typically performed via smoothing processing. In this paper, s matrices are used as submatrices to receive signals, and submatrices are shifted backward step by step to reconstruct submatrices. Then the covariance matrix is constructed and rank estimated, and the kth submatrix can be expressed as

$$X_k(t) = [x_k, x_{k+1}, \ldots, x_{k+s-1}] \tag{15}$$

Its covariance matrix can be determined as

$$\hat{R}_k = X_k(t) * X_k^H(t)/Nr = R_k + R_N \tag{16}$$

where Nr is the number of snapshots; $R_k = AE\left[D_k(t) * D_k^H(t)\right] A^H$ represents the covariance matrix corresponding to the source; $R_N = \sigma^2 I$ is the noise covariance matrix; and σ^2 is the noise power. It is easy to verify that if $\lambda_1 \geq \lambda_2 \geq \ldots \geq \lambda_k = \ldots \lambda_M = 0$ is the M eigenvalues of the matrix R and $\mu_1 \geq \mu_2 \geq \ldots \geq \mu_k \geq \ldots \geq \mu_M$ is the M eigenvalues of the matrix $\hat{R}$, then $\mu_m = \lambda_m + \sigma^2$, $m \in [1,M]$ can be obtained. In the smoothing processing, the covariance matrix constructed by all submatrices is superimposed, and the mean value is taken. Then the eigenvalue decomposition is carried out. Therefore, the number of large eigenvalues of the covariance matrix $\hat{R}$ and the number of signal sources can be determined as k, so as the recovery order of the AR model. The specific flow chart of the proposed algorithm is shown in Fig. 2.

4. SIMULATION RESULT

In order to analyse the performance of the proposed algorithm, in this section, the simulation results that the desired signal is preprocessed by the CZT and the 6-point Sinc interpolation are compared to verify the performance of the KT transform and analyze their computational burden, and then the AR model is applied to compensate the insufficient data of array element. Based on the above simulation, three jamming signals and noise are introduced to the received signal, and then the 6-point KT-Sinc, the KT-CZT algorithm, and the KT-CZT-AR algorithm are applied to correct the AFT. Finally, the adaptive beamforming (ADBF) performances of these three algorithms are compared and analysed.

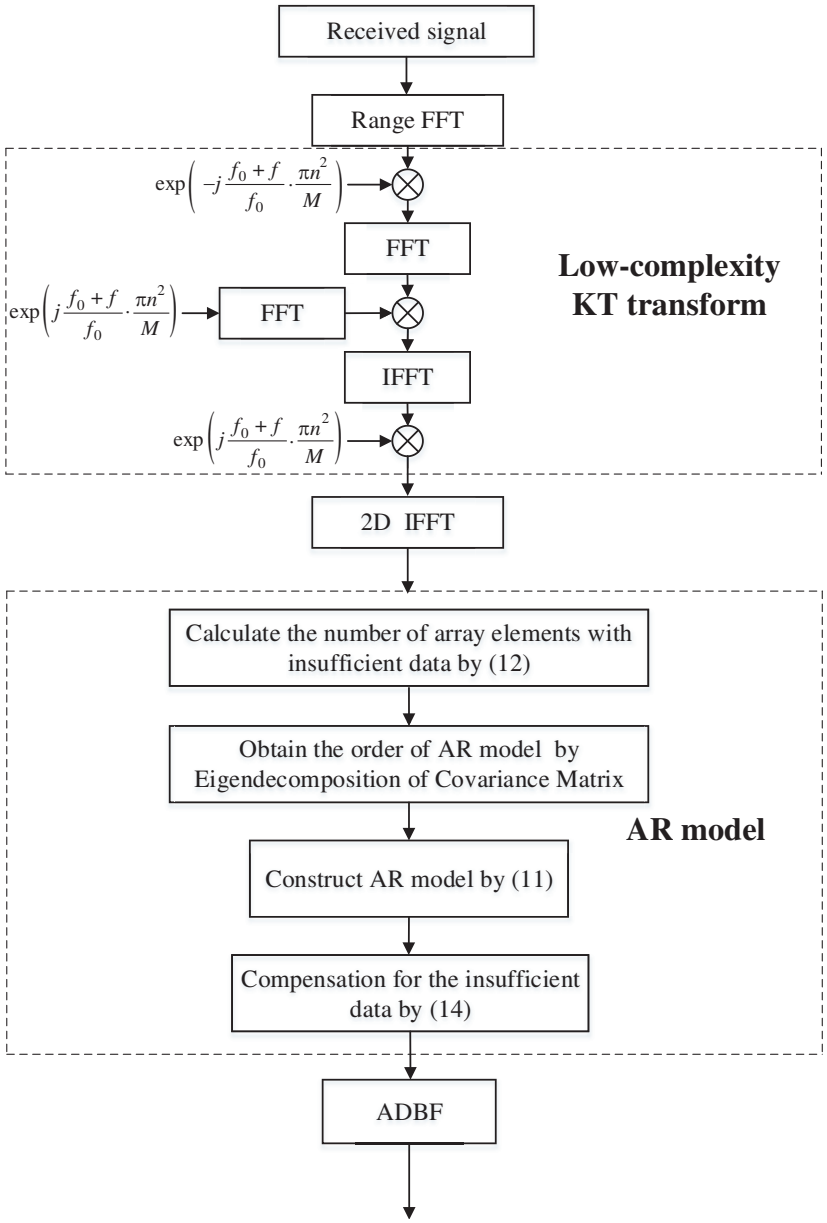

Figure 2. Flowchart of the KT-CZT-AR algorithm.

4.1. Performance Analysis

In this section, a half-wavelength ULA model is established, and the LFM signal is used as the wideband array of the target signal. The simulation parameters are shown in Table 1.

The first simulation experiment validates the superior performance of the KT transform based on CZT in correcting the AFT. As depicted in Fig. 3(a), the wideband aperture effect results in the range-compressed signal, after matched filtering, not focusing on the same range cell. Furthermore, in Fig. 4(a), the signal amplitudes of the 1st, 16th, and 32nd array elements exhibit obvious deviations in the amplitude direction. However, as illustrated in Figs. 3(b) and (c), the two different KT transforms can correct the range-compressed signal into a horizontal straight line, demonstrating the effective correction of the AFT by the KT transform. Nonetheless, after the received signal is processed by the KT-Sinc in Fig. 4(b), insufficient data is observed at both ends of the array element, and this issue can be effectively improved using CZT.

Table 1. Simulation parameter table.

Parameter	Value
Carrier frequency	1000 MHz
Bandwidth	400 MHz
Sampling frequency	500 MHz
Number of array elements	32
Direction of the target source	$-10°$
Direction of the interference sources	$-4°$ $20°$ $50°$
Input SNR of each frequency point	$15 \sim 30$ dB
Input INR of each frequency point	30 dB

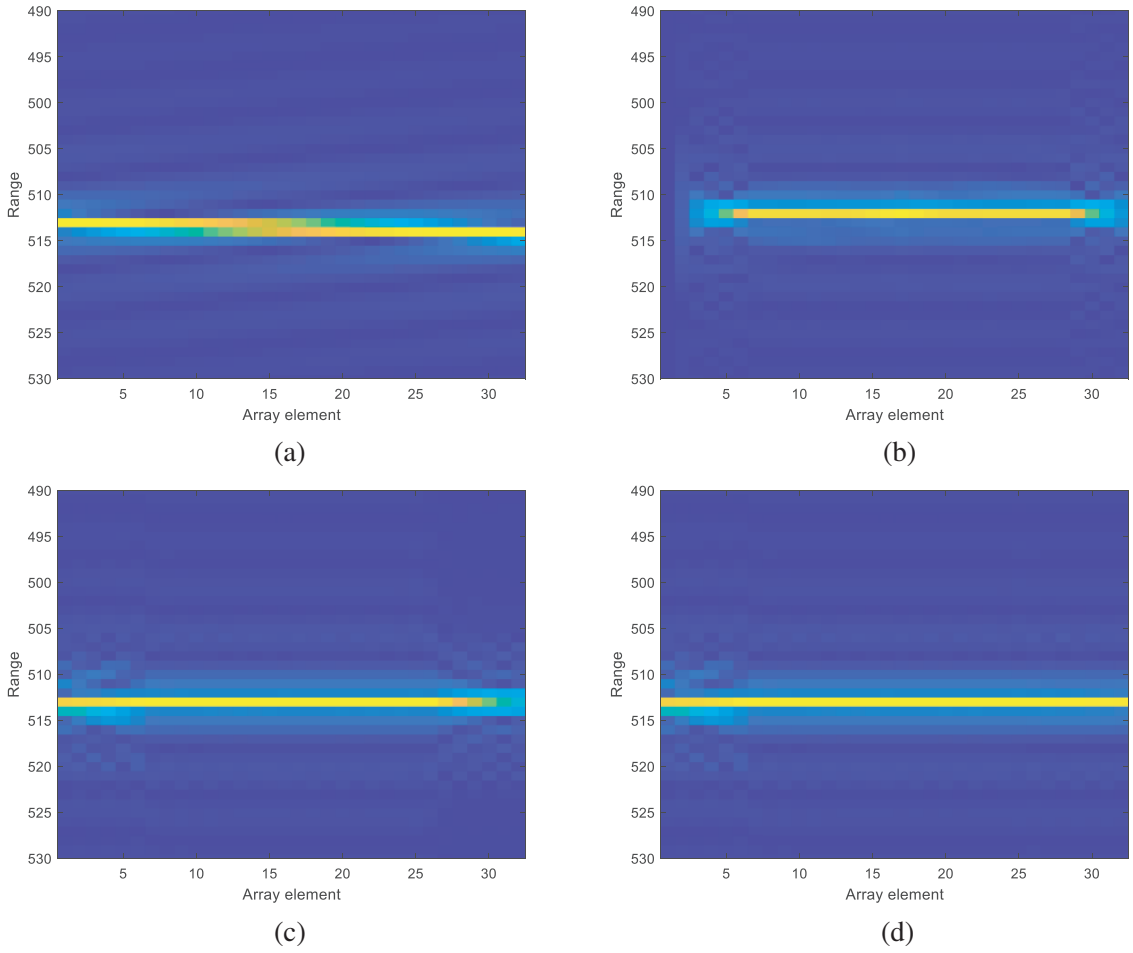

Figure 3. Range-compressed signal: (a) Before KT, (b) KT-Sinc, (c) KT-CZT, (d) KT-CZT-AR.

As shown in Fig. 3(c) and Fig. 4(c), although the signal amplitude of the edge element corrected by the CZT has been significantly improved, there still exists a significant gap compared with the center array element. Additionally, the covariance matrix is constructed by using the desired signal, and its characteristic decomposition is carried out. From the large eigenvalue and the number of sources, the recovery order of AR model can be determined as 1. Therefore, the problem of insufficient data of the

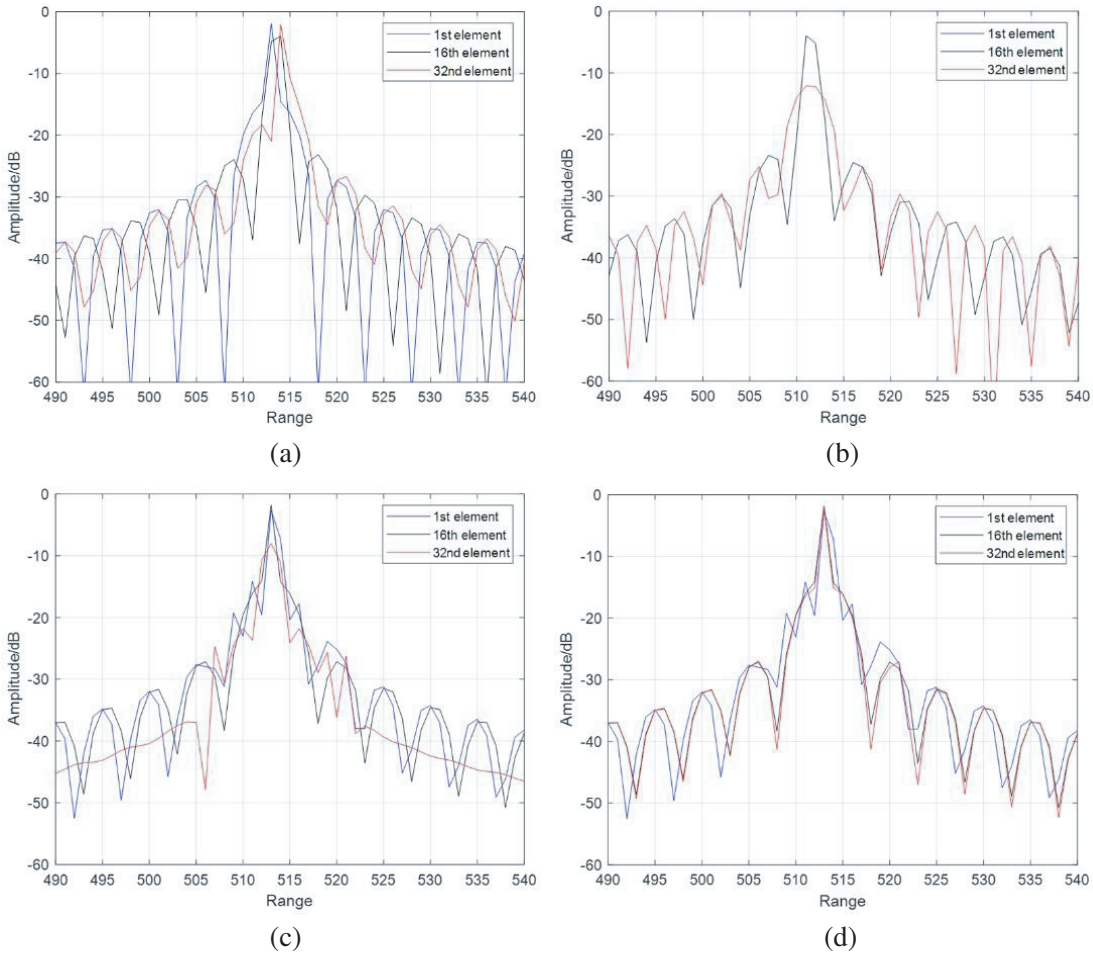

Figure 4. Amplitudes of different array elements: (a) Before KT, (b) KT-Sinc, (c) KT-CZT, (d) KT-CZT-AR.

range-compressed signal in Fig. 3(d) is compensated by using the AR model to predict the data of edge elements. It can be seen from Fig. 4(d) that the amplitude of the edge array element is no different from the center array element. Therefore, the algorithm proposed in this paper can not only correct the AFT, but also effectively solve the defects of the conventional KT algorithm.

In the subsequent experiment, three wideband jamming signals and channel noise from Table 1 are incorporated into the simulation. The received signals are corrected and compensated for the aperture effect using the aforementioned three algorithms, and then beamforming is performed. In order to ensure the validity of the simulation experiments, the covariance matrices of the three methods are all calculated in the time domain. Meanwhile, since the wideband array system will simultaneously receive the target signal, jamming signals, and the noise, after the eigen-decomposition of the covariance matrix is used to determine the recovery order of the AR model, the traditional linearly constrained minimum variance (LCMV) method is used for beamforming. The process of the LCMV algorithm can be expressed as follows

$$w = \frac{R_j^{-1} a}{a^H R_j^{-1} a} \tag{17}$$

where w represents the spatial adaptive weight vector, R_j the interference sample covariance matrix, and a the steering vector.

In order to recover the array element data, the covariance matrix is constructed by the sampled signal of 15 elements in front of the element which have the problem of insufficient data. As shown in

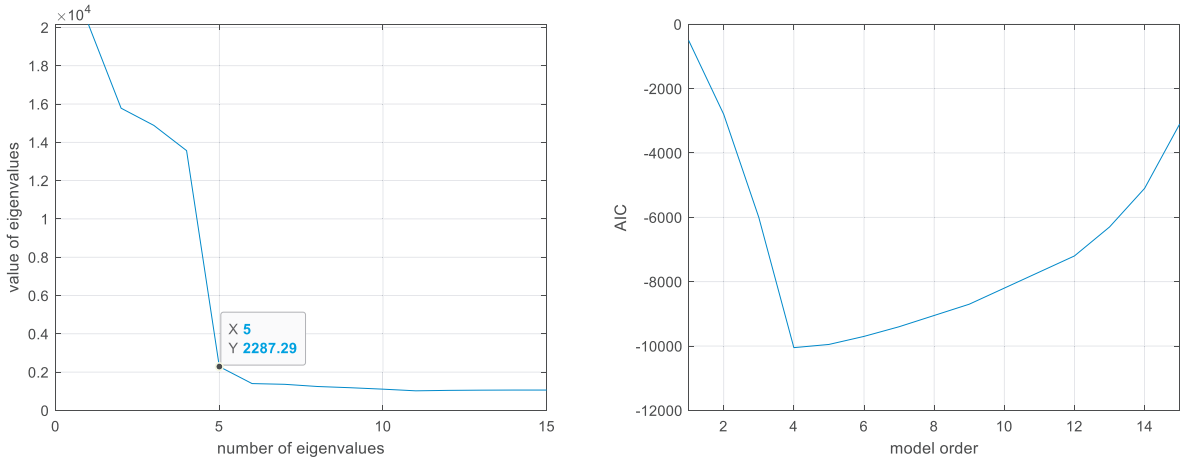

Figure 5. The modified AIC criterion: (a) Eigenvalues of the covariance matrix, (b) AIC of different orders.

Fig. 5(a), the number of large eigenvalues of the covariance matrix is 4, which is consistent with the number of input sources in this simulation. Meanwhile, the value of the AIC criterion is the lowest at 4 points in Fig. 5(b), thus the proposed method for estimating the order of the AR model is feasible.

Table 2 shows the results of ADBF using different methods after the received signal is preprocessed by the KT transform. When the input interference to noise ratio (INR) is fixed at 15 dB, the effect of changing the input signal to noise ratio (SNR) on the performance of the three algorithms is analysed. Theoretically, the output signal to interference plus noise ratio (SINR) after beamforming should be linear with the input SNR. As shown in Table 2, the output SINR of the three KT algorithms clearly conforms to this rule, and the output SINR of the proposed algorithm is improved by about 2 dB compared with the KT-Sinc algorithm and about 1 dB compared with the CZT. Therefore, the algorithm proposed in this paper can not only effectively correct the AFT but also significantly improve the performance of ADBF.

Table 2. Output SINR with input INR fixed at 30 dB.

Input SNR/dB	Output SINR/dB		
	KT-Sinc	KT-CZT	KT-CZT-AR
15	27.7295	28.2910	29.4386
20	32.6849	33.1037	34.3202
25	37.4720	38.3424	39.2114
30	42.3883	43.1390	44.6072

4.2. Computational Analysis

Table 3 shows the computational complexity of the different methods. Assuming that the number of range cells is Nr, and the number of array elements is M, thus the input signal is a matrix with Nr rows and M columns. If the computational complexity is only considered from the perspective of floating-point operations, the computational complexity of the Sinc interpolation is $O(NrM \log_2 M)$. However, it is also necessary to find the position of the new element sampling point in the original sampling point when performing interpolation. The binary search algorithm is the method with the lowest time complexity, and the time complexity of $Nr \times M$ searches is $O(NrM \log_2 M)$. The time complexity of searching the new sampling points considers the number of times that the two real numbers are

Table 3. Computational complexity analysis.

Method	matrix dimension	computational complexity
Sinc	$Nr \times M$	$O\left(NrM \log_2 M\right)$
The binary search algorithm	$Nr \times M$	$O\left(NrM \log_2 M\right)$
CZT	$Nr \times M$	$O\left(NrM \log_2 \left(2M-1\right)\right)$

compared. Compared with the comparison of real numbers, the digital signal processor is better at floating-point operations, so the process of searching will take more time. Meanwhile, different range cells have different interpolation coefficients, and each coefficient needs to be stored in the hardware processing. Then the interpolation process is performed, so it will take more time, and it is difficult to implement in hardware.

However, when the circular fast convolution of the CZT is used to realize the linear convolution, the signal needs to be filled with zeros. Therefore, for the data of $Nr \times M$, the lowest value of its computational complexity is $O\left(NrM \log_2 \left(2M-1\right)\right)$. When the number of array elements is higher, the efficiency of the KT-CZT is higher than KT-Sinc, and the computational complexity is also lower. The real advantage of the KT-CZT is still that FFT and IFFT can be used instead of convolution, which is more efficient and more suitable for modern DSP hardware.

5. CONCLUSION

This paper proposes a low-complexity KT algorithm based on the CZT and AR model. According to the inherent characteristics of the two-dimensional signal of the wideband receiving array, the KT algorithm is introduced into a wideband system to eliminate the influence of the AFT. Then the model of the KT-CZT algorithm is constructed, which improves the computational efficiency of the algorithm. Finally, in order to compensate the insufficient data of the array element inherent in the KT transform, AR model is used to compute the insufficient data of the signal in the two-dimensional time domain, which significantly improves the output SINR of ADBF. The effectiveness of the algorithm is verified by the simulation results.

ACKNOWLEDGMENT

This work was partly supported by the National Natural Science Foundation of China [No. 61771182, No. 62271190], Natural Science Foundation of Jiangsu Province of China [BK20221499], and Science and Technology on Electronic Information Control Laboratory.

REFERENCES

1. Wang, J., D.-D. Cai, and F. Yang, "Aperture effect influence and analysis of wideband phased array radar," *Procedia Engineering*, Vol. 29, 1298–1303, 2012.
2. Zhu, X. and Z. Kai, "A study on compensation of aperture fill time based on frequency-shifting," *IET International Radar Conference*, 2013.
3. Zhang, C. and Q. Lai, "Research on phased array radar affected by aperture fill time," *Journal of Microwave Science*, Vol. 33, No. 4, 67–69, 2017.
4. Wen, S., Q. Yuan, and E. Mao, "Digital compensation of aperture crossing time for wideband phased array radar Stretch processing," *Journal of Electronics*, Vol. 33, No. 6, 961–964, 2005.
5. Frost, III, O. L., "An algorithm for linearly constrained adaptive array processing," *Proc. IEEE*, Vol. 60, No. 8, 926–935, 1972.
6. Hoffman, A. and S. M. Kogon, "Subband STAP in wideband radar systems," *Proceedings of the 2000 IEEE Sensor Array and Multichannel Signal Processing Workshop. SAM 2000 (Cat. No. 00EX410)*, 256–260, IEEE, 2000.

7. Godara, L. C., "Application of the fast fourier transform to broadband beamforming," *Journal of the Acoustical Society of America*, Vol. 98, No. 1, 230–240, 1995.
8. Bao, Z., M. Xing, and T. Wang, *Radar Imaging Technology*, Beijing Publishing House of Electronics Industry, 2005
9. Yi, H., C. Y. Fan, J. G. Yang, et al., "Imaging and locating multiple ground moving targets based on Keystone transform and FrFT for single channel SAR system," *2nd Asian-Pacific Conference on Synthetic Aperture Radar (APSAR 2009)*, 2009.
10. Jiao, Z. and W. Zhang, "A novel detection method based on generalized Keystone transform and RFT for high-speed maneuvering target," *International Symposium on Computational Intelligence and Design (ISCID)*, Hangzhou, China, 2015.
11. Candocia, F. and J. C. Principe, "Comments on "Sinc interpolation of discrete periodic signals"," *IEEE Transactions on Signal Processing*, Vol. 46, No. 7, 2044–2047, 1998.
12. Çulha, O. and Y. Tanik, "Low complexity Keystone transform and radon fourier transform utilizing chirp-z transform," *IEEE Access*, Vol. 8, 105535–105541, 2020.
13. Zhu, D. and Z. Zhu, "Range resampling in the polar format algorithm for spotlight SAR image formation using the chirp z-Transform," *IEEE Transactions on Signal Processing*, Vol. 55, No. 3, 1011–1023, 2007.
14. Wang, T. T., "The segmented chirp Z-transform and its application in spectrum analysis," *IEEE Transactions on Instrumentation and Measurement*, Vol. 39, No. 2, 318–323, 1990.
15. Liu, G., Y. Liu, C. Li, and X. Chen, "Weighted multisteps adaptive autoregression for seismic image denoising," *IEEE Geoscience and Remote Sensing Letters*, Vol. 15, No. 9, 1342–1346, 2018.
16. Lu, J., Z. Xi, and M. Zhang, "MTD processing based on Keystone transform for LFMCW radar," *Electronic and Automation Control Conference (IMCEC)*, Xi'an, China, 2016.
17. Jiang, Y., M. Shen, and G. Han, "An efficient ADBF algorithm based on Keystone transform for wideband array system," *Progress In Electromagnetics Reacher Letters*, Vol. 102, No. 20, 167–175, 2022.
18. Qian, Y., R. Yan, and S. Hu, "Bearing degradation evaluation using recurrence quantification analysis and kalman filter," *IEEE Transactions on Instrumentation and Measurement*, Vol. 63, No. 11, 2599–2610, 2014.
19. Goto, S., M. Nakamura, and K. Uosaki, "On-line spectral estimation of nonstationary time series based on AR model parameter estimation and order selection with a forgetting factor," *IEEE Transactions on Signal Processing*, Vol. 43, No. 6, 1519–1522, 1995.